Risk Analysis, Vol. 24, No. 1, 2004

Estimating Contaminant Dose for Intermittent Dermal Contact: Model Development, Testing, and Application

W. J. Riley,[1] T. E. McKone,[2] and E. A. Cohen Hubal[3]

Assessments of aggregate exposure to pesticides and other surface contamination in residential environments are often driven by assumptions about dermal contacts. Accurately predicting cumulative doses from realistic skin contact scenarios requires characterization of exposure scenarios, skin surface loading and unloading rates, and contaminant movement through the epidermis. In this article we (1) develop and test a finite-difference model of contaminant transport through the epidermis; (2) develop archetypal exposure scenarios based on behavioral data to estimate characteristic loading and unloading rates; and (3) quantify 24-hour accumulation below the epidermis by applying a Monte Carlo simulation of these archetypal exposure scenarios. The numerical model, called Transient Transport through the epiDERMis (TTDERM), allows us to account for variable exposure times and time between exposures, temporal and spatial variations in skin and compound properties, and uncertainty in model parameters. Using TTDERM we investigate the use of a macro-activity parameter (cumulative contact time) for predicting daily (24-hour) integrated uptake of pesticides during complex exposure scenarios. For characteristic child behaviors and hand loading and unloading rates, we find that a power law represents the relationship between cumulative contact time and cumulative mass transport through the skin. With almost no loss of reliability, this simple relationship can be used in place of the more complex micro-activity simulations that require activity data on one- to five-minute intervals. The methods developed in this study can be used to guide dermal exposure model refinements and exposure measurement study design.

KEY WORDS: Dermal exposure; intermittent exposures; pesticide exposure; surface contact

1. INTRODUCTION

Quantifying dermal uptake from contacts with contaminated surfaces in residential environments requires the ability to model intermittent contacts. In realistic exposure scenarios, surface contact times and times between contacts are highly variable for both adults and children. Videotapes of children's activities over extended periods[1,2] reveal that surface contact rates can be higher than 1 min^{-1}. Furthermore, not all contacts involve contaminated surfaces; some contacts lead to loading while others lead to unloading of contaminants from the skin surface. Compounding this temporal complexity in skin-surface boundary conditions are temporal and spatial variability of skin properties of a particular individual, variability between individuals, and uncertainty and variability in chemical properties.

Fig. 1 presents an approach and outlines the important steps required to estimate dermal uptake resulting from contact with pesticide-contaminated surfaces. The approach begins by quantifying the amount of pesticide applied in the building. The next step is to estimate, based on the application type and amount,

[1] Earth Sciences Division, 90-1106, 1 Cyclotron Road, Lawrence Berkeley National Lab, Berkeley, CA 94720.
[2] Energy Environment Technology Division, 90-3058, 1 Cyclotron Road, Lawrence Berkeley National Lab, Berkeley, CA 94720 and School of Public Health, U.C. Berkeley.
[3] U.S. EPA, National Exposure Research Laboratory.

0272-4332/04/0100-0073$22.00/1 © 2004 Society for Risk Analysis

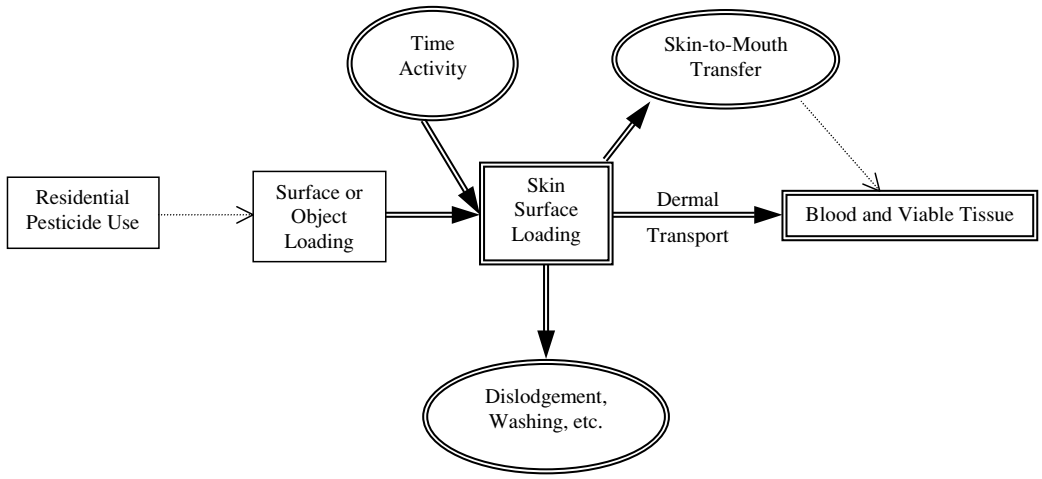

Fig. 1. Components of the modeling steps necessary to predict dermal uptake of a skin contaminant. In this article we address the components shown with double lines.

the household surface loading. Using time-activity data and estimates of loading efficiency, the skin-surface loading can be estimated. Once the chemical is present on the skin surface it can be dislodged, washed off, transferred to the mouth, or moved through the epidermis into the blood stream. In this article we describe the development and application of a general approach to address the steps shown in double lines in Fig. 1.

The transfer of chemicals from household surfaces to skin surface and into viable tissues and blood depends on two classes of exposure factors: (1) those factors that determine the loading and retention of chemical substances on the skin surface as a result of contact with surfaces (Table I) and (2) those factors that determine the quantity of chemical transferred from the skin surface to viable tissue and the blood stream.[3] Loading and retention factors include characteristics of the surface, skin, and contaminant; contact mechanics; and environmental conditions. Uptake factors include characteristics of the skin; characteristics of the chemical, vehicle, and matrix on the skin surface; and skin exposure conditions.

Historically, two approaches, referred to as the micro-activity and macro-activity approaches, have been applied to model dermal and nondietary ingestion exposure.[4] In the micro-activity approach, exposure is modeled as a series of transfers or removals resulting from discrete contact events (e.g., right hand contacting toy for 10 seconds, fingers

Table Ia. Exposure Factors that Impact the Loading and Retention of Chemical Substances on the Skin

Factor	Examples
Form of the contamination	Residue, particle, formulation, age, physicochemical properties
Surface characteristics	Hard, plush, porous, surface loading, previous transfer
Skin characteristics	Moisture, age, loading, previous transfer
Contact mechanics	Pressure, duration, smudge, repetition
Environmental conditions	Temperature, relative humidity, air exchange

Table Ib. Exposure Factors that Impact the Quantity of Chemical Transferred from the Surface of the Skin to Viable Tissue and Blood Stream

Factor	Examples
Chemical-specific properties	Partition coefficients, polarity, chemical structure, molecular weight, volatility, binding capacity in SC, metabolic capacity in VE
Skin-specific factors	Exposure site, skin age, skin condition, hydration, circulation to skin, skin temperature
Chemical, vehicle, and matrix characteristics	Residue, particle bound, formulation, release rate of pesticide from vehicle
Skin exposure	Pesticide loading on skin, concentration at skin surface, multiple versus single-dose application, residence time on skin, skin surface area

contacting mouth for 3 seconds). In the macro-activity approach, dermal exposure is modeled using empirically derived transfer coefficients to lump the mass transfer associated with a series of contact events. Until about 1995, research on dermal exposure focused on chemical uptake from relatively long-term exposures or for single contact events. In response to the Food Quality Protection Act's requirement to assess cumulative pesticide exposures, dermal exposure methods over the last several years have shifted to characterize micro-activities that include intermittent dermal loading and retention. Unfortunately, the dermal dose models have not been updated to match this ongoing research; this lack motivated us to develop the tools described here.

In vitro experiments with skin diffusion cells have demonstrated that, under steady-state conditions, the rate of chemical flux through the skin, F_{ss} (μg m^{-2} s^{-1}), from a chemical concentration in a solvent vehicle on the skin surface is proportional to the skin mass-transfer coefficient, U (m s^{-1}), a skin-to-vehicle (e.g., water) partition coefficient, K_m (–), and the chemical concentration in the vehicle on the skin surface, C_v (μg m^{-3}):[6]

$$\begin{aligned} F_{ss} &= U K_m C_v \\ &= \frac{D}{l} K_m C_v, \end{aligned} \tag{1}$$

where the mass transfer coefficient U is approximated by the ratio $\frac{D}{l}$ under steady-state conditions; D is the effective skin diffusion coefficient (m^2 s^{-1}), often taken as the stratum corneum (SC) diffusion coefficient; and l is the SC thickness (m). The relationship between the skin mass-transfer coefficient and skin and compound properties has been addressed by many studies.[7–12] Johnson *et al.*[13] examined the added complication that, in real skin, steady-state transport through the stratum corneum (SC) is a combination of trans, lateral, and vertical between-cell diffusion. They showed that diffusion within the SC has a strong dependence on molecular size for small solutes and a weak size dependence for larger solutes.

In their comprehensive review of skin permeability, Scheuplein and Blank[5] point out that the "barrier" function of the epidermis resides almost entirely in the SC and that, for low molecular weight electrolytes, the SC has about 1,000 times the diffusive resistance of underlying skin layers. In addition, they note that (1) the SC is always partially hydrated with a water content on the order of 15% to 50%; (2) the lipid solubility of a chemical plays a crucial role in determining its transport rate through the SC; (3) measurements of skin permeability made *in vitro* can differ significantly from those made *in vivo*; and (4) the effective diffusion coefficient through the SC is on the order of 10^{-13} to 10^{-14} m^2 s^{-1} for low molecular weight compounds and 10^{-15} to 10^{-17} m^2 s^{-1} for higher molecular weight compounds.

Available dermal uptake models are based on steady state permeability,[14,15] estimates of cumulative mass uptake from short-term loading from contact with soil or during showers,[16,17] analytical transient models for single-contact events,[18–22] and numerical solutions to single-contact events.[23] To simplify analyses, steady-state conditions for dermal absorption are often assumed when conducting dermal risk assessments.[9,12] However, both theoretical[16,18,19] and experimental studies[22,24,25] reveal that mass flux from vehicle into skin is greater than steady-state estimates when contact times are short. While the analytical models are appropriate for single-contact events, they are unable to predict contaminant uptake resulting from a series of intermittent exposures. Predicting the long-term cumulative mass flux through the epidermis for multiple contacts of variable duration requires a spatially and temporally resolved numerical model. To our knowledge the model by Roy *et al.*[23] represents the sole example of this approach in the literature, although these authors did not apply their model to intermittent contacts. The ability to accurately estimate uptake from intermittent contacts remains a critical and missing link in pesticide risk assessments.[4,26] This issue is particularly relevant for children, who are an important focus of studies addressing cumulative pesticide exposure.

Several recent experiments have highlighted the differences between steady and nonsteady uptake scenarios. For example, using a series of short-term experiments with *in vitro* uptake of trichloroethylene by human skin from a water vehicle, Bogen *et al.*[24] showed that the flux of contaminant through the skin per contact time increases with decreasing contact time. This result is expected since the concentration gradient at the skin surface decreases as the skin approaches steady state, thereby reducing the driving force for flux into the skin. Pirot *et al.*[22] report on the use of attenuated-total-reflectance Fourier-transform-infrared spectroscopy (ATR-FTIR) to rapidly quantify *in vivo* the uptake of 4-cyanophenol into human SC. They applied this technique to estimate the permeability coefficient and to calculate the time required to achieve maximum flux through the skin. McDougal

and Jurgens-Whitehead[25] also observed, in transient diffusion cell experiments with dibromomethane in rat skin, that the linear uptake model does not accurately predict uptake for relatively short exposure times.

Here we propose a general approach to predict cumulative dermal uptake based on (1) archetypal micro-activity patterns; (2) Monte Carlo sampling and modeling of archetypal exposure scenarios; and (3) a macroscopic characteristic of the long-term exposure (i.e., cumulative contact time). Note that we focus here on modeling the chemical transfer from the skin surface through the viable epidermis and into blood under conditions where skin loading and properties are changing on relatively short time scales. We do not address the relationship between concentrations on household surfaces and concentrations on the skin surface, which has been addressed elsewhere.[4]

We expect significant variation in contact times and surface concentrations for realistic scenarios of dermal contact with contaminated surfaces. Thus, the concentration on the skin surface that drives uptake can be quite variable on the time scale of transport through the SC and VE. This variability leads to a number of questions that cannot be answered by previously published models: When is a non-steady-state analysis required to accurately predict cumulative uptake? How does cumulative uptake depend on cumulative exposure time? How does the dependence of cumulative uptake versus contact time vary with compound or matrix properties? We illustrate here the applicability of our general approach to addressing intermittent contacts in risk assessments and in designing future experiments.

In the following sections we develop, evaluate, and apply a numerical model, Transient Transport through the epiDERMis (TTDERM), of transient contaminant transport through the skin driven by fluctuating skin-surface boundary conditions. As demonstrated below, this approach is fundamentally distinct from the common practice of applying a single-contact model for each contact. The model allows the user to define skin and contaminant properties (e.g., spatially dependent diffusion coefficients, skin partition coefficients, and thickness of the SC and viable epidermis (VE)) that can impact contaminant accumulation below the VE. TTDERM solves the transient diffusion equation to determine the contaminant concentration profile within the skin and mass flux across the skin boundaries. In Section 2 we (1) describe the relationships and assumptions used to develop TTDERM; (2) evaluate TTDERM's predictions of contaminant dose against analytical solutions for single-contact events; and (3) describe the development of eight-hour archetypal exposure scenarios based on observed children's activity patterns. In Section 3 we apply TTDERM to these exposure scenarios to investigate a macro-activity approach to estimating diurnal dermal uptake from intermittent contacts. Finally, we develop, for a specific set of compound and skin properties, a simplified contaminant uptake relationship based on cumulative contact time.

2. METHODS

2.1. Modeling Transient Contaminant Diffusion Through Skin

TTDERM uses a one-dimensional finite-difference discretization of Fick's second law to estimate the transient diffusive flux at any point in the skin. The model allows for intermittent contacts on the skin surface through boundary condition manipulation. This approach is therefore distinct from previously reported approaches that simply calculate transport through the skin for a single contact event and then sum over the number of contact events. The user defines the thickness and diffusivity of the SC and VE, and a partition coefficient is used to relate concentrations between the lower boundary of the SC and upper boundary of the VE.

As applied to the transient concentration profile within the epidermis, Fick's second law takes the form:

$$\frac{\partial C(x,t)}{\partial t} = \frac{\partial}{\partial x}\left[D(x,t)\frac{\partial C(x,t)}{\partial x}\right], \qquad (2)$$

where $C(x, t)$ is the concentration of the compound in the skin (μg m^{-3}) at distance x (m) into the skin and time t (s). To simplify the notation we replace $C(x, t)$ by C and $D(x, t)$ by D. Furthermore, we nondimensionalize Equation (2) by substituting $C' = \frac{C}{\dot{C}}$; $x' = \frac{x}{\dot{x}}$; $t' = \frac{t}{\dot{t}}$; and $D' = \frac{D}{\dot{D}}$, to obtain

$$\frac{\partial C'}{\partial t'} = \frac{\partial}{\partial x'}\left[D'\frac{\partial C'}{\partial x'}\right]. \qquad (3)$$

For the simulations presented here, $\dot{C}$ is taken as the skin-surface concentration, $\dot{x}$ is taken to be 1 μm, $\dot{D}$ is the diffusivity in the stratum corneum, and $\dot{t} = \frac{\dot{x}^2}{\dot{D}}$. For notational simplicity, we drop the superscript primes in Equation (3) for the remainder of the article.

We discretize Equation (3) separately in the SC and VE using a Crank–Nicholson approach,[27] which is second-order accurate in space and time. Twenty

Table II. Boundary Conditions for the Numerical Model under the Presence or Absence of Contaminant on the Skin Surface

Scenario	Boundary Condition	Boundary Condition
Contaminant present	Constant concentration	$C(x=0,t)=1$
Contaminant absent	Constant gradient	$\frac{\partial C}{\partial x}(x=0,t)=0$

and 100 control volumes are used in the SC and VE, respectively. The spatial discretization varies from 0.1 μm near the skin surface and SC-VE boundary to 2 μm in the center of the SC and bottom of VE. The nondimensional temporal discretization ($\Delta t'$) depends on skin properties and varies from 0.0001 to 0.01. Our method allows for a spatially and temporally dependent diffusion coefficient, variable thickness of the SC and VE, and variable spatial and temporal discretization. At the interface between the SC and VE, an equilibrium partitioning is assumed, such that

$$C(l,t) = K_{sv} C(l+\gamma, t), \tag{4}$$

where γ is the distance between the bottom control volume in the SC and the top control volume in the VE, and K_{sv} is the pollutant-dependent equilibrium partition coefficient (which ranges from ~0.1 to greater than 10,000).[9,11]

The initial condition for all the simulations is that the skin is clear of the contaminant:

$$C(x, t=0) = 0. \tag{5}$$

Equation (3) is first solved across the SC at the beginning of each time step. The boundary condition at the skin surface ($x=0$) is toggled on or off depending on whether contaminant is present on the skin surface (as noted in the scenario descriptions in Table II). The concentration boundary condition at $x=l$ is defined by Equation (4). After the SC concentration profile has been updated the flux at the bottom of the SC is calculated. Equation (3) is then solved in the VE with this flux boundary condition at $x=l+\delta$ and a constant concentration of 0 at the bottom of the epidermis ($x=L$). At the next time step, the constant concentration boundary condition at $x=l$ is re-computed assuming equilibrium partitioning, and the solution repeated.

The flux, F (μg m^{-2} s^{-1}), out of the epidermis and into the dermis is computed as

$$F = D\left(\frac{\partial C}{\partial x}\right)_{x=L}. \tag{6}$$

The total accumulated mass per skin area, M (μg m^{-2}), is

$$M = \int_0^{t_f} F \mathrm{d}t, \tag{7}$$

where t_f (s) is the time at the end of the simulation. For single-contact scenarios we evaluate the integral until M reaches 99.99% of the mass that has entered the SC; the integral is evaluated over 24 hours for the 8-hour exposure scenarios.

2.2. Analytical Solutions

We compared model predictions of the concentration profile within, and mass flux through, the skin to an analytical solution of a single-contact event. The scenario corresponds to the solution of Equation (3) with zero initial concentration throughout the skin; an imposed SC surface concentration, C_0, of 1 at $t=0$; and partitioning defined by Equation (4). Modifying the analytical solution for the analogous heat transfer problem (Carslaw and Jaeger,[28] pp. 323–324) gives, for the SC

$$C(x \le l) = \frac{C_0(k_{sv} D_s L - D_v z)}{k_{sv} D_s L + D_v l} - 2C_0 \sum_{n=1}^{\infty} \frac{\sin^2(kL\beta_n)\sin(\beta_n(l+z))}{\beta_n\left(l\sin^2(kL\beta_n) + \sigma kL \sin^2(l\beta_n)\right)} e^{-D_s\beta_n^2 t} \tag{8}$$

and for the VE

$$C(x \ge l) = \frac{k_{sv} D_s C_0 (L-z)}{k_{sv} D_s L + D_v l} - 2C_0 \sum_{n=1}^{\infty} \frac{\sin(l\beta_n)\sin(kL\beta_n)\sin(k(L-z)\beta_n)}{\beta_n\left(l\sin^2(kL\beta_n) + \sigma kL \sin^2(l\beta_n)\right)} e^{-D_s\beta_n^2 t}. \tag{9}$$

Here, $z = x - l$, $k = \sqrt{\frac{D_s}{D_v}}$, $\sigma = \frac{1}{k_{sv}}\sqrt{\frac{D_v}{D_s}}$, and D_s and D_v are the diffusivities (m^2 s^{-1}) in the SC and VE, respectively. The eigenvalues, β_n, are defined by

$$\cos(\beta l)\sin(k\beta L) + \sigma \sin(\beta l)\cos(k\beta L). \tag{10}$$

We solve for the eigenvalues by iteration.

2.3. Archetypal Exposure Scenarios

Because of the age dependencies and labor-intensive nature of gathering micro-activity data, few data sets relevant to exposure assessments currently exist. Two general approaches to gathering such data

have been used: (1) real-time hand recording, in which trained observers watch an individual and write down the information of interest on a score sheet; and (2) videotaping, in which trained videographers tape an individual and then subsequently extract the data of interest by hand or by computerized software. We used a combination of several studies to estimate contact frequencies for hand-to-surface and hand-to-mouth activity. Zartarian *et al.*[1] reported hand contact rates for four surfaces (carpet, hard floor, hard surface, and hard toys) for four children, ages 2 to 4 years, from an agricultural area of California. In this study, contact rates varied between 1 and 102 h^{-1}. Reed[2] videotaped activities of 30 children, between 18 months and 5 years old, in New Jersey for a total of 168 hours and estimated hand contact rates between 0 and 312 h^{-1} with six surfaces. Reed[2] also observed hand-to-mouth contact rates between 0 and 26 h^{-1}. Freeman *et al.*[29] reported mean hand-to-mouth contact rates ranging from 2 to 7 h^{-1}, with the rates decreasing with increasing age of the child. In the study by Tulve *et al.*[30] of 186, 69, and 117 children of ages 11 to 60, 11 to 24, and 25 to 60 months, respectively, mean hand-to-mouth rates were between 16 and 18 h^{-1}. In developing contact rates for the diurnal dermal uptake scenarios, we assumed that 50% of the contacts in any particular simulation were to contaminated surfaces.

Ivancic *et al.*[31] evaluated parameters that affect residue transfer from surface-to-skin, skin-to-other objects, and skin-to-mouth using a fluorescent tracer as a surrogate for pesticide residues. Laboratory evaluations were conducted to relate transfer of a tracer to transfer of pesticides. Parameters evaluated included: surface type, surface loading, contact motion, pressure, duration, and skin condition. Both transfers onto and off the hand were measured. We applied results from this study to estimate unloading rates from skin by surface contacts.

Table III shows the rates of loading and unloading events estimated from the above studies and applied in the diurnal archetypal exposure scenarios. The large variability in reported contact rates argues for further study to quantify this critical information for exposure assessments. In the Monte Carlo approach we apply, each 24-hour simulation is performed with loading and unloading rates defined with a normal distribution (mean, standard deviation (SD), and limit), thereby generating a wide range of contact rates. For these simulations, we take the means to be the values in the "total" columns of Table III, and we apply a SD of 50% of the mean for all parameters.

Table III. Loading, Actual Unloading, and Effective Unloading Activities

	Press	Smudge	Wash	Mouthing	Total
Loading Activities (h^{-1})	12	12			24
Actual Unloading Activities (h^{-1})	12	12	0.25	16	
Effective Activity per Actual Activity	2	2	1	2	
Effective Unloading Activities (h^{-1})	6	6	0.25	8	20

Effective unloading activities are calculated as the actual unloading rate divided by the "effective activity per activity" for each unloading behavior.

2.4. Simulations Performed

We first performed simulations of single-contact events. In each scenario the contaminant is applied to the skin for a specific contact time, t_c (s), and then removed. The relationship between contact time and mass accumulated below the skin was then determined for a range of contact times and values of K_{sv}, D_s, and D_v.

We next simulated diurnal intermittent contacts using the contact rates shown in Table III over an 8-hour period, and simulated the integrated 24-hour accumulated mass. The contact events are randomly distributed over the 8-hour period, resulting in paired sequential loading and unloading events. An example of the exposure loading and unloading events over a 2-hour period and resulting predicted contaminant concentration in the middle of the SC and VE are shown in Fig. 2 (in this example $K_{sv} = 1$, $D_s = 5 \times 10^{-13}\ m^2\ s^{-1}$, and $D_v = 5 \times 10^{-11}\ m^2\ s^{-1}$). Note that the concentration in the middle of the SC responds

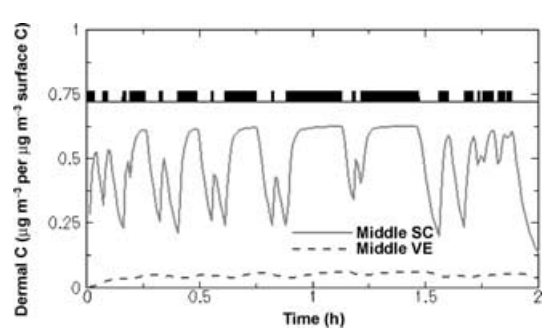

Fig. 2. Example of a 2-hour intermittent exposure scenario. Shown are the concentrations in the middle of the stratum corneum and middle of the viable epidermis for $K_{sv} = 1$, $D_s = 5 \times 10^{-13}\ m^2\ s^{-1}$, and $D_v = 5 \times 10^{-11}\ m^2\ s^{-1}$. Also shown are the time periods when contaminant is on the skin surface (solid bars).

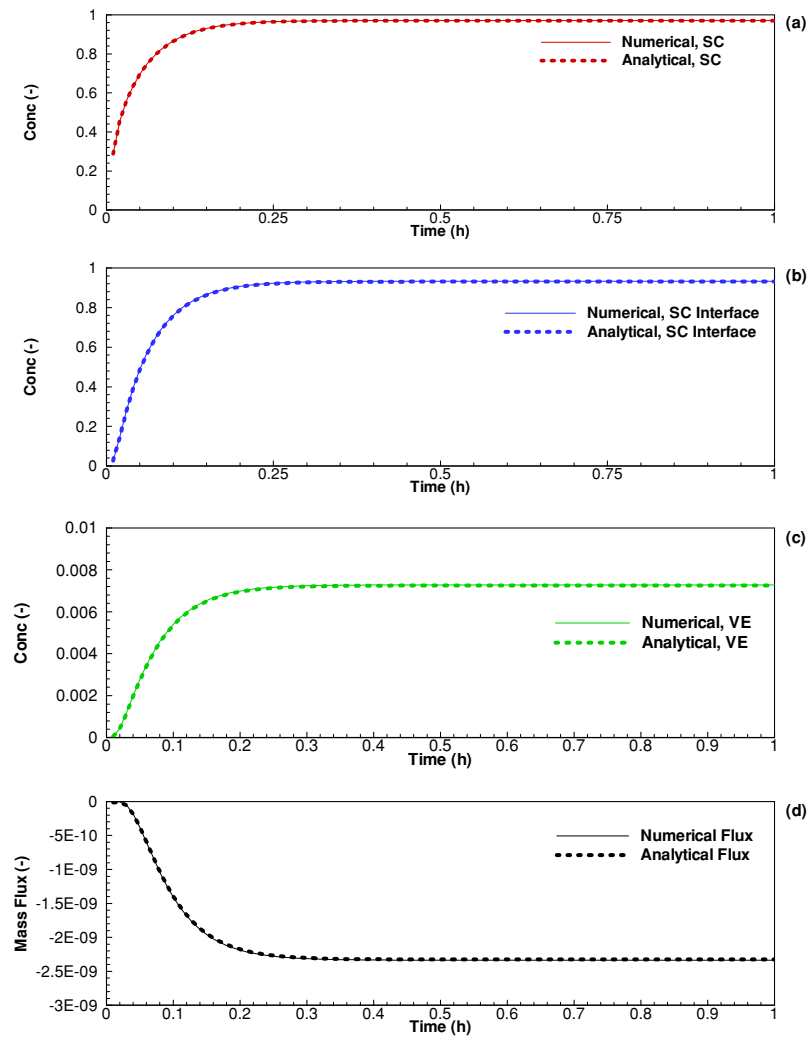

Fig. 3. Comparison between analytical solutions (dashed lines) and numerical simulations (solid lines) of skin concentrations in the (a) center of the SC, (b) interface between the SC and VE, (c) center of the VE, and (d) mass flux into the body for $K_{sv} = 100$, $D_s = 5 \times 10^{-13}$ m^2 s^{-1}, $D_v = 5 \times 10^{-11}$ m^2 s^{-1}, $l = 15\,\mu$m, and $L = 215\,\mu$m.

relatively rapidly to the contact exposure while the concentration in the middle of the VE responds more slowly. The relative magnitude of the concentration profile responses within the epidermis depends on the values of K_{sv}, D_s, and D_v.

3. RESULTS AND DISCUSSION

3.1. Model Testing

To test the numerical model, we ran TTDERM for several single-contact scenarios with values of K_{sv} between 0.1 and 1,000, and compared contaminant concentration profiles within the skin and the mass flux through the skin to the analytical solutions (Equations (8) and (9)). For these simulations we used $D_s = 5 \times 10^{-13}$ m^2 s^{-1}, $D_v = 5 \times 10^{-11}$ m^2 s^{-1}, $l = 15\ \mu$m, and $L = 215\ \mu$m. The model accurately captured the concentration profiles within the SC and VE and the mass flux out of the VE into the body (e.g., Figs. 3(a)–(c) show results for $K_{sv} = 100$).

We also compared model predictions to measurements of transient dibromomethane transport through a rat SC held in a diffusion cell.[25] TTDERM accurately predicted the reported transient mass transport through the SC and into the receptor vessel over the 20-minute experiment.

3.2. Single-Contact Simulations

Fig. 4 shows predicted mass accumulated below the skin for single-contact events of varying exposure times and values of K_{sv}, D_s, and D_v. In Table IV we list the estimated values of K_{sv}, D_s, and D_v for a set of common organophosphates, pyrethroids, and other

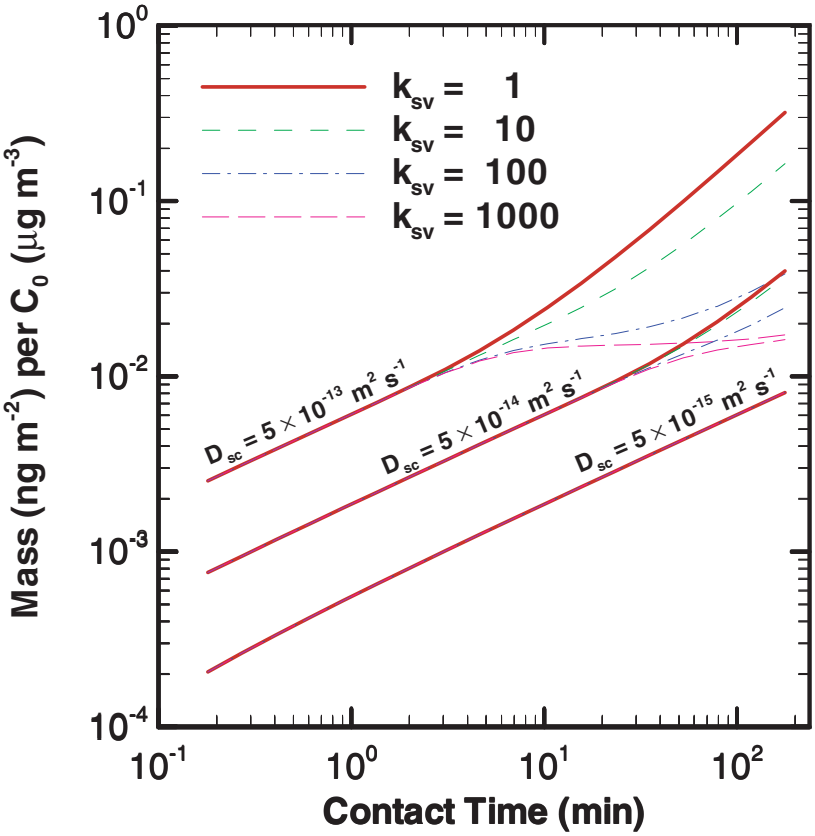

Fig. 4. Predicted mass accumulated below the epidermis for single-contact events. The mass accumulated is independent of K_{sv} below contact times of about 2, 20, and 200 minutes for $D_s = 5 \times 10^{-13}$ m^2 s^{-1}, $D_s = 5 \times 10^{-14}$m^2 s^{-1}, and $D_s = 5 \times 10^{-15}$ m^2 s^{-1}, respectively.

chemicals of interest. This table reveals both the typical range of these parameters and the range of uncertainty in estimating a derived property (e.g., D_s) that cannot be measured directly. The octanol-water partition coefficient K_{ow} and molecular weight (MW) in Table IV are from the CalTOX database.[32] We estimate the skin-water partition coefficient (K_m, which is similar to K_{sv}) using a correlation from the most recent U.S. EPA dermal guidance.[33] Because there are no experimentally confirmed methods to determine D_s we use two published estimation methods to determine this parameter. The lower D_s values are based on U.S. EPA[33] methods and the upper value is based on McKone and Howd.[12] The values of D_v are estimated using the approach of Cleek and Bunge[14] and show much less chemical-to-chemical variability than D_s.

In Fig. 4, $D_v = 5 \times 10^{-11}$ m^2 s^{-1} for all the simulations, and the three groups of curves correspond to $D_s = 5 \times 10^{-13}$ m^2 s^{-1} (the top set of curves, typical of lower molecular weight compounds, e.g., toluene or chloroform), $D_s = 5 \times 10^{-14}$ m^2 s^{-1}, and $D_s = 5 \times 10^{-15}$ m^2 s^{-1} (bottom two sets of curves, typical of higher molecular weight compounds, including organophosphates and pyrethroids). The mass accumulated is independent of K_{sv} below contact times of about 2, 20, and 200 minutes for $D_s = 5 \times 10^{-13}$ m^2 s^{-1}, $D_s = 5 \times 10^{-14}$ m^2 s^{-1}, and $D_s = 5 \times 10^{-15}$ m^2 s^{-1}, respectively. Resistance in the SC dominates the dynamic response of the mass flux through the epidermis. The characteristic time for a contaminant to move through the SC, τ (s), is[11]

$$\tau \sim \left(\frac{l^2}{6D_{sc}}\right) \tag{11}$$

For the conditions in Fig. 4, $\tau \sim 1.3$, 13, and 130 minutes for $D_s = 5 \times 10^{-13}$, 5×10^{-14}, and 5×10^{-15} m^2 s^{-1}, respectively. These values are comparable to the contact times below which the mass accumulated is independent of K_{sv}. Thus, for $t_c < \tau$ the cumulative mass uptake through the skin is insensitive to K_{sv}.

For short contact times the slope of the cumulative mass uptake line in log-log space is 0.5, which corresponds to a relationship for the mass accumulated below the skin of the form

$$M \propto t_c^{0.5}. \tag{12}$$

Table IV. Estimated SC Diffusion Coefficient for Organophosphates, Pyrethroids, and Other Chemicals

	$\log K_{ow}$[a]	MW[a] (g mol^{-1})	K_m[b]	D_s[c] (m^2 s^{-1})	D_v[d] (m^2 s^{-1})
Organophosphate pesticides					
Acephate	−1.00	183.18	0.11	6.2×10^{-15}–4.0×10^{-14}	5.2×10^{-11}
Azinphos-methyl	2.70	317.34	100	1.1×10^{-15}–6.3×10^{-14}	4.0×10^{-11}
Chlorpyrifos	4.92	350.60	6040	7.2×10^{-16}–1.2×10^{-13}	3.8×10^{-11}
Coumaphos	4.06	362.80	1230	6.1×10^{-16}–9.0×10^{-14}	3.7×10^{-11}
Diazinon	3.35	304.35	335	3.9×10^{-14}–7.9×10^{-14}	4.1×10^{-11}
Dichlorvos (DDVP)	1.47	221.00	10.5	3.8×10^{-15}–5.3×10^{-14}	4.8×10^{-11}
Disulfoton	4.02	274.38	1150	1.9×10^{-15}–1.0×10^{-13}	4.3×10^{-11}
Fenitrothion	3.40	277.25	366	1.2×10^{-15}–8.5×10^{-14}	4.3×10^{-11}
Fenthion	4.10	278.34	1340	1.2×10^{-15}–1.1×10^{-13}	4.3×10^{-11}
Malathion	2.86	330.36	136	6.2×10^{-16}–6.5×10^{-14}	3.9×10^{-11}
Oxydemeton methyl	−0.74	246.30	0.18	1.8×10^{-15}–3.2×10^{-14}	4.5×10^{-11}
Parathion	3.83	291.27	811	1.0×10^{-15}–9.5×10^{-14}	4.2×10^{-11}
Pyrethroid pesticides					
Bifenthrin	6.00	422.90	44,000	1.9×10^{-16}–1.5×10^{-13}	3.5×10^{-11}
Cypermethrin	3.83	416.30	811	2.1×10^{-16}–7.7×10^{-14}	3.5×10^{-11}
Deltamethrin	3.83	505.20	811.14	6.5×10^{-17}–6.8×10^{-14}	3.2×10^{-11}
Permethrin	3.83	391.00	811.14	2.8×10^{-16}–8.0×10^{-14}	3.6×10^{-11}
Other chemicals					
Methanol	−0.74	32.00	0.18	2.9×10^{-14}–1.1×10^{-13}	1.3×10^{-10}
Ethanol	−0.32	46.10	0.39	2.4×10^{-14}–8.6×10^{-13}	1.0×10^{-10}
Chloroform	1.97	119.40	26.30	9.4×10^{-15}–8.9×10^{-14}	6.5×10^{-11}
Toluene	2.69	92.10	99.37	1.3×10^{-14}–1.3×10^{-13}	7.4×10^{-11}

[a]CalTOX.[32]
[b]Estimated as $K_m = (2.8 \times 10^{-8}\ \mathrm{m^2\ s^{-1}\ per\ cm^2\ h^{-1}})\frac{K_p l}{D_s} = K_{ow}^{0.66}$ according to U.S. EPA recommendations,[33] where K_p is the skin permeability (cm h^{-1}).
[c]The range is based on the following models for D_s: $D_s = 2.8 \times 10^{-8}\ \mathrm{m^2\ s^{-1}\ per\ cm^2\ h^{-1}}(10^{-2.8-0.0056MW})\,l$; USEPA,[33] and $D_s = \frac{2.8 \times 10^{-8}\ \mathrm{m^2\ s^{-1}\ per\ cm^2\ h^{-1}}}{K_m MW^{0.6}}(10^{-2.8-0.0056MW})\,l = \frac{2.8 \times 10^{-8}\ \mathrm{m^2\ s^{-1}\ per\ cm^2\ h^{-1}}}{K_m MW^{0.6}}(2.4 \times 10^{-6} + 3 \times 10^{-5} K_{ow}^{0.8})$; McKone and Howd.[12]
[d]The diffusion coefficient in the viable epidermis is estimated as $D_v = \frac{7.1 \times 10^{-10}}{MW^{0.5}}$; based on Bunge and Cleek.[14]

Other investigators have observed this relationship between mass accumulated and single-contact exposure time.[25]

For long contact times (i.e., $t_c \gg \tau$), the slope of the cumulative mass uptake line in log-log space is 1. Note that in Fig. 4 this slope is not realized for the larger values of K_{sv} because the simulations end before a steady-state flux is established in the VE. The slope of 1 corresponds to the familiar steady-state condition that mass accumulates below the skin linearly with increasing contact time, i.e., $M \propto t_c$. Fig. 4 also provides an estimate of the time required for the skin to reach saturation as a function of K_{sv}. We note that the slopes for both short and long contact times are independent of skin diffusivity. Also, for long contact times (i.e., $t_c \gg \tau$), the mass accumulated becomes a strong function of K_{sv}. Increasing K_{sv} effectively reduces the driving gradient between the skin surface and the SC by increasing the concentration gradient between the SC and VE.

While the slopes of the mass uptake curve at large and small value of t_c are independent of skin and compound properties, the curve of M versus t_c is effectively shifted up or down as a function of D_s. As D_s increases the mass accumulated in the epidermis increases for the same t_c as a result of the lowered resistance to contaminant movement through the SC.

3.3. Intermittent Multiple-Contact Simulations

In this section we describe results for the archetypal 8-hour exposure scenarios described above. We emphasize that these results are from the full TT-DERM solution, and are therefore different (and more realistic) than would be calculated by summing the mass accumulated below the epidermis from a series of single-contact events. Model predictions of total mass accumulated (M) over the 24-hour period as a function of cumulative contact time, T (h), are shown in Figs. 5(a)–(c). Each panel shows M for

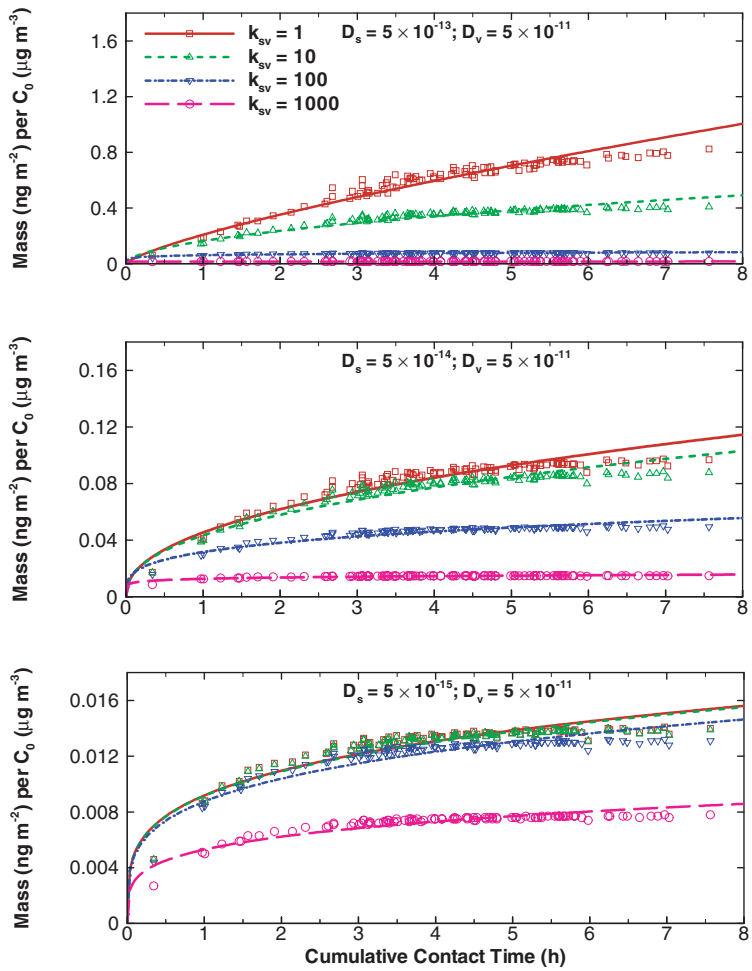

Fig. 5. Monte Carlo simulations of total mass accumulated over the 24-hour period as a function of total contact time. Each point represents a separate 24-hour simulation. Each panels shows results for $K_{sv} = 1$, 10, 100, and 1,000, and the effective diffusivity of the VE, D_v, is constant at 5×10^{-11} m^2 s^{-1}. The effective SC diffusivity, D_s, varies for each panel: (a) $D_s = 5 \times 10^{-13}$ m^2 s^{-1}; (b) $D_s = 5 \times 10^{-14}$ m^2 s^{-1}; and (c) $D_s = 5 \times 10^{-15}$ m^2 s^{-1}.

$K_{sv} = 1, 10, 100$, and 1,000; D_v is the same for all cases (5×10^{-11} m^2 s^{-1}). The panels differ in their stratum corneum diffusivity (D_s): (a) 5×10^{-13}, (b) 5×10^{-14}, and (c) 5×10^{-15} m^2 s^{-1}. Each point on these figures corresponds to a separate 24-hour simulation. The variability in M for a particular set of properties and value of T results from the imposed random timing of contact events and range of loading and unloading rates, as described in Table III and illustrated in Fig. 2. For equivalent T, scenarios with more uniformly distributed contact events will result in larger values of M than scenarios with contacts that are more "bunched" in time. Contacts that occur soon (with respect to τ) after a previous contact event will result in lower mass flux into the skin, since the concentration gradient at the skin surface will be relatively lower.

Cumulative mass uptake M is about an order of magnitude lower for each order of magnitude lower SC diffusivity. Further, the lower SC diffusivity decreases distinctions between mass uptake at different values of K_{sv} as a result of the relatively larger resistance imposed by lower SC diffusivity.

The lines shown in Figs. 5(a)–(c) correspond to least-squares power-law curve fits to the individual 24-hour cumulative mass uptakes:

$$M = cT^b. \tag{13}$$

This power-law relationship is consistent with the notion that the rate of change of M decreases with increasing T. With increasing T the likelihood that subsequent contacts are impacted by residual contaminant in the skin increases. Residual contaminant in the skin will result in lower mass uptake than would be expected for an isolated single contact of equivalent contact time. The power-law curve fits the data well for cumulative contact times below about 6 hours, after which increasing T has a relatively smaller impact on cumulative uptake than predicted by the curve fit.

For particular values of D_s and D_v the relationship between M and T depends strongly on K_{sv}. This

Table V. Power-Law Curve Fit Parameters Corresponding to Equation (13)

	$D_s = 5 \times 10^{-13}$ m^2 s^{-1}		$D_s = 5 \times 10^{-14}$ m^2 s^{-1}		$D_s = 5 \times 10^{-15}$ m^2 s^{-1}	
K_{sv}	b	c	b	c	b	c
1	0.76	0.21	0.45	0.046	0.26	0.0092
10	0.53	0.16	0.42	0.043	0.25	0.0092
100	0.15	0.061	0.27	0.032	0.25	0.0087
1000	0.022	0.016	0.10	0.013	0.23	0.0053

dependence is strongest when D_s is largest because of the relative resistive impact of D_s compared to K_{sv}. Larger values of K_{sv} effectively reduce the contaminant flux from the SC into the VE, thereby reducing the driving concentration gradient across the skin surface, i.e., $\frac{\partial C}{\partial x}$ $(x = 0)$. This reduced gradient results in a reduced mass flux into the SC.

3.4. Simple Cumulative Mass Uptake Relationship

There is currently no simple algorithm available in the literature to estimate cumulative mass uptake for realistic intermittent contacts over the course of a day. The results presented in Figs. 5 (a)–(c) indicate that a simple model can capture the cumulative mass uptake through the skin as a result of a series of intermittent contacts over an 8-hour period. Table V gives the constants characterizing each of the six lines in Figs. 5 (a)–(c). Note that the values of b and c and the residual differences between the power-law curve fits and simulation predictions will be functions of D and K_{sv}. Future work will apply the methods and models developed here to elucidate these dependencies over a range of skin and compound properties.

4. CONCLUSIONS

Current dermal uptake models rely on steady-state uptake (permeability) algorithms or assume single-contact exposures. Steady-state permeability models are valid only after the skin is saturated with the contaminant and are inaccurate for short and intermittent contact scenarios. More complex analytical models that simulate transient uptake during single contacts cannot be applied to situations where there are multiple surface loading and unloading events. These issues motivated our efforts to develop a numerical model (TTDERM) for transient and intermittent dermal contact events. We successfully tested TTDERM against analytical solutions of single-contact exposure scenarios for a range of compound properties.

For single-contact exposures we demonstrated that mass uptake is proportional to (1) the square root of contact time for short contacts and (2) the contact time for long contacts. Between these extremes a more complicated relationship exists, as illustrated in Fig. 4. For a particular set of values for D_s and D_v and short contact time $(t_c < \tau)$ the mass uptake is independent of K_{sv}, while for long contacts $(t_c \gg \tau)$ mass uptake depends strongly on K_{sv}.

We also demonstrated that 24-hour cumulative mass uptake following an 8-hour period of randomly occurring intermittent exposures can be approximated with a simple power-law relationship that depends on cumulative contact time. The constants defining these power-law relationships depend on the skin properties K_{sv}, D_s, and D_v. Our results indicate that increasing the partition coefficient between the SC and VE (K_{sv}) decreases the cumulative mass transferred through the VE. This effect is caused by increased levels of residual contaminant in the SC that reduces the concentration gradient driving transport from the skin surface into the SC for subsequent contacts. Because of this "residual effect," simply summing the mass uptake for a series of "clean-skin" single-contact estimates cannot accurately capture integrated dose over an exposure period with multiple contacts. The extent to which the single-contact estimate differed from the true dose varies with contaminant and skin properties. These results demonstrate that accurately predicting cumulative contaminant uptake through the skin under realistic exposure scenarios requires the ability to simulate a series of intermittent short-term contacts.

In spite of much recent progress, there are a number of modeling issues that remain before we can accurately assess human exposures to pesticides in residences. Specifically, we need to better characterize (1) the composition and properties of residues in the environment; (2) how these factors change with time; (3) people's behavior leading to surface contacts (e.g., number of hand contacts per hour with contaminated and uncontaminated surfaces); and (4) how these

factors affect loading and unloading from the skin surface. Improvements in our understanding of these issues can significantly improve our estimates of cumulative contaminant transport through the epidermis for realistic exposure scenarios.

ACKNOWLEDGMENTS

This work was supported in part by the U.S. Environmental Protection Agency National Exposure Research Laboratory through Interagency Agreement DW-988-38190-01-0 and carried out at Lawrence Berkeley National Laboratory through the U.S. Department of Energy under Contract Grant No. DE-AC03-76SF00098.

NOMENCLATURE

b, c	power-law curve-fit parameters
C	concentration of the compound in the skin (μg m^{-3})
C_v	chemical concentration in the vehicle on the skin surface (μg m^{-3})
C_0	SC skin-surface concentration (μg m^{-3})
$\dot{C}$	characteristic surface concentration (μg m^{-3})
D	effective skin diffusion coefficient (m^2 s^{-1})
$\dot{D}$	characteristic diffusivity (m^2 s^{-1})
D_s, D_v	diffusivities in the SC and VE, respectively (m^2 s^{-1})
F	flux out of the epidermis (μg m^{-2} s^{-1})
F_{ss}	steady-state flux through the skin (μg m^{-2}s^{-1})
k	constant in the analytical solution
K_m	skin-to-vehicle partition coefficient
K_{ow}	octanal-water partition coefficient
K_p	skin permeability (cm h^{-1})
K_{sv}	equilibrium partition coefficient between the SC and VE
l, L	thickness of the SC and epidermis (m)
M	total accumulated mass per skin area (μg m^{-2})
MW	molecular weight (g mol^{-1})
t	time (s)
$\dot{t}$	characteristic time (s)
T	total contact time (h)
t_c	contact time (s)
t_f	time at the end of the simulation (s)
$\Delta t'$	nondimensional temporal discretization
U	skin mass-transfer coefficient (m s^{-1})
x	distance into the skin (m)
$\dot{x}$	characteristic length (1 μm)
z	constant in the analytical solution

Greek Letters

β_n	eigenvalues
γ	distance between the bottom control volume in the SC and the top control volume in the VE (m)
$\Delta\dot{t}$	temporal discretization
τ	characteristic time for a contaminant to move through the SC (s)
σ	constant in the analytical solution

REFERENCES

1. Zartarian, V. G., Ferguson, A. C., & Leckie, J. O. (1997). Quantified dermal activity data from a four-child pilot field study. *Journal of Exposure Analysis and Environmental Epidemiology*, *7*, 543–552.
2. Reed, K. (1998). *Quantification of Children's Hand and Mouthing Activities Through a Videotaping Methodology*. Camden, NJ: Rutgers University and UMDNJ-Robert Wood. Johnson Medical School.
3. Hubal, E. A. C., Sheldon, L. S., Burke, J. M., McCurdy, T. R., Barry, M. R., Rigas, M. L., Zartarian, V. G., & Freeman, N. C. G. (2000). Children's exposure assessment: A review of factors influencing children's exposure, and the data available to characterize and assess that exposure. *Environmental Health Perspectives*, *108*, 475–486.
4. Zartarian, V. G., Ozkaynak, H., Burke, J. M., Zufall, M. J., Rigas, M. L., & Furtaw, E. J. (2000). A modeling framework for estimating children's residential exposure and dose to chlorpyrifos via dermal residue contact and nondietary ingestion. *Environmental Health Perspectives*, *108*, 505–514.
5. Scheuplein, R. J., & Blank, I. H. (1971). Permeability of skin. *Physiological Review*, *51*, 702–747.
6. Kasting, G. B., Smith, R. L., & Cooper, E. R. (1987). Effect of lipid solubility and molecular size on percutaneous absorption. *Pharmacological Skin*, *1*, 138–153.
7. Michaels, A. S., Chandrasekaren, S. K., & Shaw, J. E. (1975). Drug permeation through human skin: Theory and in vitro experimental measurement. *AIChE J*, *21*, 985–996.
8. Albery, W. J., & Hadgraft, J. (1979). Percutaneous absorption: Theoretical description. *Journal of Pharmacy and Pharmacology*, *31*, 140–147.
9. U.S. EPA. (1992). *Dermal Exposure Assessment: Principles and Applications*. Washington, DC: Office of Health and Environmental Assessment, U.S. EPA.
10. Potts, R. O., & Guy, R. H. (1992). Predicting skin permeability. *Pharmacological Research*, *9*, 663–669.
11. Flynn, G. L. (1990). Physicochemical determinants of skin absorption. In T. R. Gerity & C. J. Henry (Eds.), *Principles of Route-to-Route Extrapolation for Risk Assessment* (pp. 93–127). New York: Elsevier.
12. McKone, T. E., & Howd, R. A. (1992). Estimating dermal uptake of nonionic organic chemicals from water and soil: 1. Unified fugacity-based models for risk assessments. *Risk Analysis*, *12*, 543–557.
13. Johnson, M. E., Berk, D. A., Blankschtein, D., Golan, D. E., Jain, R. K., & Langer, R. S. (1996). Lateral diffusion of small

compounds in human stratum corneum and model lipid bilayer systems. *Biophysical Journal*, *71*, 2656–2668.
14. Bunge, A. L., & Cleek, R. L. (1995). A new method for estimating dermal absorption from chemical exposure. 2. Effect of molecular weight and octanol water partitioning. *Pharmaceutical Research*, *12*, 88–95.
15. Frasch, H. F. (2002). A random walk model of skin permeation. *Risk Analysis*, *22*, 265–276.
16. McKone, T. E. (1993). Linking a Pbpk model for chloroform with measured breath concentrations in showers—Implications for dermal exposure models. *Journal of Exposure Analysis and Environmental Epidemiology*, *3*, 339–365.
17. Shatkin, J. A., Wagle, M., Kent, S., & Menzie, C. A. (2002). Development of a biokinetic model to evaluate dermal absorption of polycyclic aromatic hydrocarbons from soil. *Human and Ecological Risk Assessment*, *8*, 713–734.
18. Cleek, R. L., & Bunge, A. L. (1993). A new method for estimating dermal absorption from chemical exposure. 1. General approach. *Pharmaceutical Research*, *10*, 497–506.
19. McCarley, K. D., & Bunge, A. L. (1998). Physiologically relevant one-compartment pharmacokinetic models for skin. 1. Development of models. *Journal of Pharmaceutical Sciences*, *87*, 470–481.
20. McCarley, K. D., & Bunge, A. L. (2000). Physiologically relevant two-compartment pharmacokinetic models for skin. *Journal of Pharmaceutical Sciences*, *89*, 1212–1235.
21. McCarley, K. D., & Bunge, A. L. (2001). Pharmacokinetic models of dermal absorption. *Journal of Pharmaceutical Sciences*, *90*, 1699–1719.
22. Pirot, F., Kalia, Y. N., Stinchcomb, A. L., Keating, G., Bunge, A., & Guy, R. H. (1997). Characterization of the permeability barrier of human skin in vivo. *Proceedings of the National Academy of Sciences of the United States of America*, *94*, 1562–1567.
23. Roy, A., Weisel, C. P., Lioy, P. J., & Georgopoulos, P. G. (1996). A distributed parameter physiologically-based pharmacokinetic model for dermal and inhalation exposure to volatile organic compounds. *Risk Analysis*, *16*, 147–160.
24. Bogen, K. T., Keating, G. A., Meissner, S., & Vogel, J. S. (1998). Initial uptake kinetics in human skin exposed to dilute aqueous trichloroethylene in vitro. *Journal of Exposure Analysis and Environmental Epidemiology*, *8*, 253–271.
25. McDougal, J. N., & Jurgens-Whitehead, J. L. (2001). Short-term dermal absorption and penetration of chemicals from aqueous solutions: Theory and experiment. *Risk Analysis*, *21*, 719–726.
26. Zartarian, V. G., & Leckie, J. O. (1998). Dermal exposure: The missing link. *Environmental Science & Technology*, *32*, A134–A137.
27. Press, W., Flannery, B., Teukolsky, S., & Vetterling, W. (1989). *Numerical Recipes (FORTRAN)* (p. 702). Cambridge: Cambridge University Press.
28. Carslaw, H. S., & Jaeger, J. C. (1986). *Conduction of Heat in Solids*, 2nd ed. (p. 510). Oxford: Clarendon Press.
29. Freeman, N. C. G., Jimenez, M., Reed, K. J., Gurunathan, S., Edwards, R. D., Roy, A., Adgate, J. L., Pellizzari, E. D., Quackenboss, J., Sexton, K., & Lioy, P. J. (2001). Quantitative analysis of children's microactivity patterns: The Minnesota children's pesticide exposure study. *Journal of Exposure Analysis and Environmental Epidemiology*, *11*, 501–509.
30. Tulve, N. S., Suggs, J. C., McCurdy, T., Hubal, E. A. C., & Moya, J. (2002). Frequency of mouthing behavior in young children. *Journal of Exposure Analysis and Environmental Epidemiology*, *12*, 259–264.
31. Ivancic, W., Nishioka, M., Barnes, R., & Hubal, E. C. (submitted for publication). Development and evaluation of a quantitative video fluorescence imaging system and fluorescent tracer for measuring transfer of pesticide residues from surfaces to hands with repeated contacts.
32. CalTOX. (2001). The CalTOX database is available for download at http://eetd.lbl.gov/ied/ERA/.
33. U.S. EPA. (2001). *Risk Assessment Guidance for Superfund Volume I: Human Health Evaluation Manual (Part E, Supplemental Guidance for Dermal Risk Assessment, Appendix A)*. Washington, DC: Office of Emergency and Remedial Response, U.S. Environmental Protection Agency.